



OPEN

DATA DESCRIPTOR

Geopositioning time series from offshore platforms in the Adriatic Sea

Mimmo Palano¹✉, Giuseppe Pezzo²✉, Enrico Serpelloni², Roberto Devoti², Nicola D'Agostino², Stefano Gandolfi³, Federica Sparacino¹, Letizia Anderlini⁴, Luca Poluzzi³, Luca Tavasci³, Paolo Macini³, Grazia Pietrantonio², Federica Riguzzi², Ilaria Antoncecchi^{5,6}, Francesco Ciccone^{5,7}, Giada Rossi^{5,6}, Antonio Avallone² & Giulio Selvaggi²

We provide a dataset of 3D coordinate time series of 37 continuous GNSS stations installed for stability monitoring purposes on onshore and offshore industrial settlements along a NW-SE-oriented and ~100-km-wide belt encompassing the eastern Italian coast and the Adriatic Sea. The dataset results from the analysis performed by using different geodetic software (Bernese, GAMIT/GLOBK and GIPSY) and consists of six raw position time series solutions, referred to IGB08 and IGS14 reference frames. Time series analyses and comparisons evidence that the different solutions are consistent between them, despite the use of different software, models, strategy processing and frame realizations. We observe that the offshore stations are subject to significant seasonal oscillations probably due to seasonal environmental loads, seasonal temperature-induced platform deformation and hydrostatic pressure variations. Many stations are characterized by non-linear time series, suggesting a complex interplay between regional (long-term tectonic stress) and local sources of deformation (e.g. reservoirs depletion, sediment compaction). Computed raw time series, logs files, phasor diagrams and time series comparison plots are distributed via PANGAEA (<https://www.pangaea.de>).

Background & Summary

We present the results from the analysis of a new dataset of GNSS stations installed on onshore and offshore industrial settlements provided by Eni S.p.A. (<https://www.eni.com>). This is one of the research activities started by INGV in the framework of the program “CLYPEA: Innovation network for future energy”, as part of the “sub-soil deformations” project¹. Such a dataset has been collected at continuous GNSS stations installed, respectively closely to 13 onshore infrastructures (e.g. storage centers) located along the Italian Adriatic coast and 24 offshore hydrocarbon production platforms anchored to the seabed in central and northern Adriatic Sea (Fig. 1a).

This dataset improves the current density of GNSS stations along the Adriatic coastal belt, allowing also to capture local and/or regional crustal deformation on a large sector of the northern Adriatic Sea, therefore representing a potentially invaluable dataset, although it involves GNSS stations not realized for geophysical purposes. Moreover, due to its offshore extension, the dataset must be considered as unique since until now, with the exclusion of very few GNSS stations (such as the HARV station installed on the Harvest platform, approximately located 10 km off the coast of central California²), not so extensive offshore datasets have been publicly released.

The raw GNSS dataset covers a period ranging from 1998 to the end of 2017, with time series covering time spans from 0.71 to 19.08 years (Table 1 and Fig. 1b). Raw data were provided by Eni S.p.A. in the RINEX format

¹Istituto Nazionale di Geofisica e Vulcanologia, Osservatorio Etneo - Sezione di Catania, P.zza Roma 2, I-95125, Catania, Italy. ²Istituto Nazionale di Geofisica e Vulcanologia, Osservatorio Nazionale Terremoti, Via di Vigna Murata 605, I-00143, Rome, Italy. ³University of Bologna, Department of Civil, Chemical, Environmental and Materials, Engineering (DICAM), Viale Risorgimento 2, Bologna, I-40136, Italy. ⁴Istituto Nazionale di Geofisica e Vulcanologia, Sezione di Bologna, Via Donato Creti, 12, Bologna, I-40128, Italy. ⁵Ministero dello Sviluppo Economico - DGISSEG, Via Molise 2, I-00187, Rome, Italy. ⁶Research on Energy System RSE S.p.A., Via Rubattino 54, I-20134, Milano, Italy. ⁷Istituto di Scienze Marine, Consiglio Nazionale delle Ricerche, Via P. Gobetti 101, I-40129, Bologna, Italy. ✉e-mail: mimmo.palano@ingv.it; giuseppe.pezzo@ingv.it

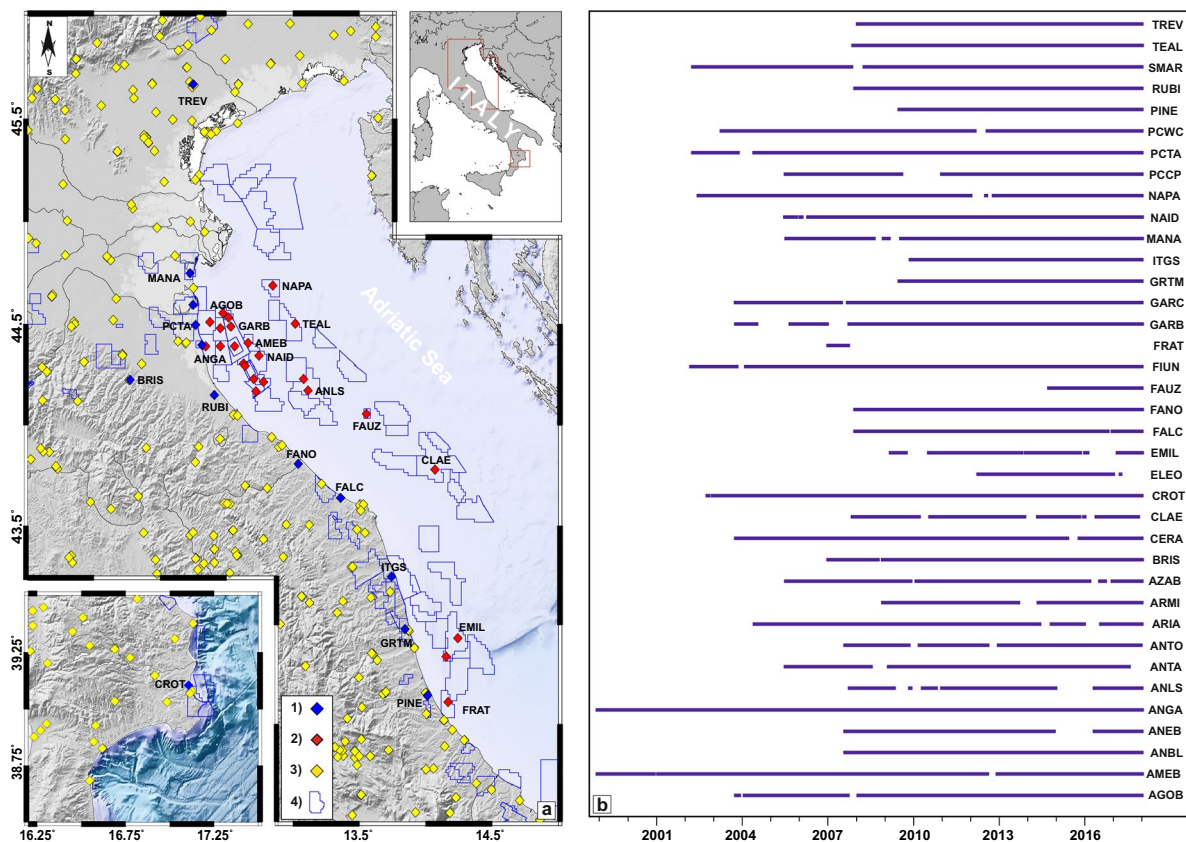


Fig. 1 (a) Map distribution of the continuous GNSS stations provided by Eni S.p.A. Legend: 1) GNSS stations installed on storage and treatment centers, 2) GNSS stations installed on offshore platforms, 3) continuous GNSS stations developed and managed by different local, national and international Institutions and Agencies (INGV, ASI, ITALPOS, NETGEO, etc), 4) Oil/Gas prospection and production concession. (b) Temporal raw data availability of the GNSS dataset (see Table 1 for additional details).

with 30-second sampling rate and containing 24 hours (00:00–23:59 UTC) of continuous tracking of NAVSTAR GPS (NAVigation Satellite Timing And Ranging Global Positioning System) satellites. In addition, Eni S.p.A. provided also a few ancillary information related to adopted receiver and antenna models and their changes over the acquisition time.

Here we provide 3D coordinate time series on a daily basis, as processed by different data analysis centers, providing a robust validation of this particular set of positions time series. Coordinates are consistent with IGB08³ and IGS14⁴ reference frames. Both reference frames have origin coinciding with the Earth system center of mass, however, the IGS14 and the IGB08 represent the GNSS realization of the ITRF2014⁵ and ITRF2008⁶ reference frames, respectively. The data files are distributed in text ASCII format (i.e. the “pos” format⁷, realized by the Plate Boundary Observatory for GNSS time series solutions sharing) via a web-based online repository.

Methods

This section illustrates the analyses carried out by different data processing centers, which analyzed the same dataset by means of different geodetic software and, within the same software adopted different procedures for the reference frames realization. With the aim of producing the most accurate final computation and, at the same time, obtaining a comparable analysis strategy, each data analysis center processed the raw GNSS data by using (i) a double difference approach, applied using the Bernese software, (ii) a double-difference distributed approach, applied by means of the GAMIT/GLOBK software package and (iii) a Precise Point Positioning (PPP) approach, applied by means of GIPSY.

The GNSS raw dataset has been processed at four different analysis centers:

- Istituto Nazionale di Geofisica e Vulcanologia - Sezione di Bologna (hereinafter INGV-BO); this analysis center provided 1 solution processed with GAMIT/GLOBK and QOCA (named *IBO_GAMIT*).
- Istituto Nazionale di Geofisica e Vulcanologia - Osservatorio Etno (hereinafter INGV-OE); this analysis center provided 1 solution processed with GAMIT/GLOBK (named *IOE_GAMIT*).
- Istituto Nazionale di Geofisica e Vulcanologia - Osservatorio Nazionale Terremoti (hereinafter INGV-ONT); this analysis center provided 1 solution processed with GIPSY (named *ONT_GIPSY*) and 1 solution processed with Bernese (named *ONT_BERNESE*).

| Site | Name | Note | Long. (°) | Lat. (°) | Height (meters) | Starting | Duration (years) |
|------|---------------------|------|-----------|----------|-----------------|----------|------------------|
| AGOB | AGOSTINO-B | P | 12.472 | 44.554 | 67.13 | 2003.78 | 14.22 |
| AMEB | AMELIA-B | P | 12.662 | 44.407 | 73.26 | 1998.92 | 19.08 |
| ANBL | ANNABELLA | P | 13.079 | 44.229 | 76.63 | 2007.60 | 10.40 |
| ANEB | ANEMONE-B | P | 12.705 | 44.229 | 63.54 | 2007.60 | 10.40 |
| ANGA | ANGELA-ANGELINA | P | 12.344 | 44.391 | 73.34 | 1998.92 | 19.08 |
| ANLS | ANNALISA | P | 13.114 | 44.171 | 63.08 | 2007.76 | 10.24 |
| ANTA | ANTARES | P | 12.454 | 44.390 | 73.11 | 2005.52 | 12.03 |
| ANTO | ANTONELLA | P | 12.777 | 44.214 | 68.06 | 2007.60 | 10.37 |
| ARIA | ARIANNA-A | P | 12.628 | 44.306 | 68.84 | 2004.42 | 13.58 |
| ARMI | ARMIDA | P | 12.453 | 44.480 | 73.03 | 2008.92 | 9.07 |
| AZAB | AZALEA-B | P | 12.720 | 44.167 | 78.15 | 2005.53 | 12.47 |
| BRIS | BRISIGHELLA | STC | 11.774 | 44.225 | 220.68 | 2007.00 | 11.00 |
| CERA | CERVIA-A | P | 12.639 | 44.294 | 67.14 | 2003.78 | 14.22 |
| CLAE | CLARA-EST | P | 14.072 | 43.780 | 65.87 | 2007.85 | 10.02 |
| CROT | CROTONE | STC | 17.106 | 39.105 | 45.78 | 2002.77 | 15.23 |
| ELEO | ELEONORA | P | 14.156 | 42.840 | 72.53 | 2012.26 | 4.99 |
| EMIL | EMILIO | P | 14.243 | 42.935 | 66.18 | 2009.19 | 8.81 |
| FALC | FALCONARA | STC | 13.358 | 43.640 | 46.38 | 2007.95 | 10.05 |
| FANO | FANO | STC | 13.041 | 43.809 | 51.39 | 2007.94 | 10.06 |
| FAUZ | FAUZIA | P | 13.554 | 44.056 | 67.00 | 2014.74 | 3.26 |
| FIUN | FIUMI UNITI | STC | 12.316 | 44.397 | 43.59 | 2002.20 | 15.80 |
| FRAT | FRATELLO CLUSTER | P | 14.168 | 42.612 | 63.69 | 2007.00 | 0.71 |
| GARB | GARIBALDI-B | P | 12.532 | 44.487 | 66.39 | 2003.77 | 14.23 |
| GARC | GARIBALDI-C | P | 12.515 | 44.531 | 72.60 | 2003.77 | 14.23 |
| GRTM | GROTTAMMARE | STC | 13.845 | 42.980 | 70.57 | 2009.50 | 8.50 |
| ITGS | ITALGAS | STC | 13.744 | 43.245 | 105.91 | 2009.92 | 8.08 |
| MANA | MANARA | STC | 12.226 | 44.750 | 44.19 | 2005.53 | 12.47 |
| NAID | NAIDE | P | 12.745 | 44.343 | 62.33 | 2005.49 | 12.51 |
| NAPA | NAOMI-PANDORA | P | 12.847 | 44.689 | 68.83 | 2002.46 | 15.53 |
| PCCP | PORTO CORSINI M E C | P | 12.561 | 44.391 | 71.99 | 2005.52 | 12.48 |
| PCTA | SPINARONI | STC | 12.267 | 44.495 | 45.16 | 2002.28 | 15.72 |
| PCWC | PORTO CORSINI M W C | P | 12.373 | 44.509 | 72.42 | 2003.27 | 14.73 |
| PINE | PINETO | STC | 14.014 | 42.644 | 55.97 | 2009.50 | 8.50 |
| RUBI | RUBICONE | STC | 12.409 | 44.150 | 47.30 | 2007.95 | 10.05 |
| SMAR | SMARLACCA | STC | 12.247 | 44.594 | 44.43 | 2002.28 | 15.72 |
| TEAL | TEA-LAVANDA-ARNICA | P | 13.019 | 44.501 | 66.16 | 2007.88 | 10.12 |
| TREV | TREVISIO | STC | 12.246 | 45.668 | 69.71 | 2008.04 | 9.96 |

Table 1. GNSS dataset provided by Eni S.p.A. For each station, site id, denomination, notes (P, Platform; STC; Storage and treatment center), coordinates, installation date and duration are reported.

- Dipartimento di Ingegneria Civile, Chimica, Ambientale e dei Materiali - Università di Bologna (hereinafter DICAM-UniBO); this analysis center provided 1 solution processed with GIPSY (named *UBO_GIPSY*) and 1 solution processed with GAMIT/GLOBK (named *UBO_GAMIT*).

In the following, a brief description of each adopted procedure for obtaining daily positions is provided. Table 2 resumes some relevant characteristics of each processing scheme, including specific models applied in the analysis.

Raw data processing by using the Bernese software. The Bernese⁸ GNSS software is a scientific, high-precision, multi-GNSS data processing software developed at the Astronomical Institute of the University of Bern. Data processing with version 5.0 of this software package was performed at INGV-ONT. Daily solutions of station positions were estimated in loosely constraint reference systems. The raw observations were processed forming Ionosphere Free linear combinations and solving for the troposphere biases and phase ambiguities using the Quasi Ionosphere-free approach⁹. The troposphere modeling consisted in an a priori dry-Niell model fulfilled by the estimation of zenith delay corrections at 1-hour intervals at each site using the wet-Niell mapping function (see Table 2). In addition, one horizontal gradient parameter per day at each site was estimated. Ocean loading was computed using the FES2004 tidal model coefficients as provided by the Ocean Tide Loading provider (<http://holt.oso.chalmers.se/loading>). The GPS orbits and the Earth's orientation parameters were fixed to the final IGS

| Solution | UBO_GAMIT | UBO_GIPSY | IBO_GAMIT | IOE_GAMIT | ONT_GIPSY | ONT_BERNESE |
|---|--|--|---------------------------------|--|---|------------------------------|
| Data processing parameters | | | | | | |
| Software | Gamit (Ver. 10.61) | GipsyX (Ver. rc0.4) | Gamit (Ver. 10.70) + QOCA | Gamit/Globk (Ver. 10.70) | Gipsy (ver. 6.3) | Bernese (ver 5.0) |
| Processing sampling rate | 30 sec | 300 sec | 30 sec | 30 sec | 30 sec | 30 sec |
| Elevation mask | 10° | 10° | 10° | 10° | 0° | 10° |
| Antenna phase center models | igs08.atx | igs14_www.atx | igs08.atx | igs14_www.atx | igs14_www.atx | igs08.atx |
| GPS orbits | IGS, final | JPL, final | IGS, final | IGS, final | JPL, final | repro2, IGS, final |
| Ocean tides loading model | FES2004 | FES2004 | FES2004 | FES2004 | FES2004 | FES2004 |
| Tropospheric mapping function | VMF1 | VMF1 | VMF1 | VMF1 | VMF1 | NIELL |
| Ionosphere correction | 2nd order ionosphere correction | 2nd order ionosphere correction | 2nd order ionosphere correction | 2nd order ionosphere correction | 2nd order ionosphere correction | no 2nd order correction |
| Ambiguity resolution | Yes | Yes, with wlpb files | Yes | Yes | Yes, with wlpb files | Yes |
| Reference frame/system and strategy for alignment of solutions | | | | | | |
| Alignment strategy | 7 parameter transformation | 7 parameter transformation | 7 parameter transformation | 7 parameter transformation | 7 parameter transformation | 4 parameter transformation |
| Reference frame/system | IGb08 | IGb08 | IGb08 | IGb08 | IGS14 | IGb08 |
| Sinex file | IGb08.snrx | IGb08.snrx | IGb08.snrx | IGb08.snrx | | IGb08.snrx |
| Reference stations | BUCU, GRAS, GRAZ, MATE, MEDI, NOT1, SOFI, WTZR, ZIMM | BUCU, GRAS, GRAZ, MATE, MEDI, NOT1, SOFI, WTZR, ZIMM | IGb08 core sites | BRUS, BRUX, COMO, GENO, GRAS, GRAZ, JOZE, MATE, NOT1, PRAT, TORI, ZIMM, ZOUF | 132 stations used for reference frame alignment | 45 anchor stations in Europe |

Table 2. Data processing parameters adopted during the processing of the GNSS dataset provided by Eni S.p.A.

products and the site coordinates were constrained to an a priori sigma of 10 m, thus the daily coordinates were estimated in a loosely constrained, unknown reference frame. In order to express the *ONT_BERNESE* solution in a unique reference frame, the daily covariance was first projected imposing tight internal constraints (at millimeter level), and then the coordinates were transformed into the ITRF2008 reference frame by a 4-parameter Helmert transformation (translations and scale factor). The regional reference frame transformation used 45 anchor sites among the IGB08 stations, located on the Eurasian Plate (see Table 2).

Raw data processing by using the GAMIT/GLOBK software. GAMIT/GLOBK¹⁰ is a GNSS analysis package, designed to run under any UNIX operating system and developed at the Massachusetts Institute of Technology (MIT), the Harvard-Smithsonian Center for Astrophysics, Scripps Institution of Oceanography and Australian National University. This software was adopted at DICAM-UniBO (version 10.61) and at INGV-BO and INGV-CT (version 10.7). All the three analysis centers adopted the IGS “Repro2 campaign”¹¹ standards during the raw dataset processing. In this step, INGV-CT and DICAM-UniBO included into the cluster processing some high-quality IGS¹² stations (Table 2) in order to improve the overall configuration of the network and to tie the regional stations to an external global reference frame. The INGV-BO solution is part of a continental-scale geodetic analysis, including >3000 continuous GNSS stations^{13,14}. Because of this large number of sites, the GAMIT analysis was performed independently for several sub-networks, each made by <50 stations, with each sub-network sharing a set of high-quality IGS stations, which are used as tie-stations in the combination step.

During the processing step, the GAMIT software uses an ionosphere-free linear combination of GNSS phase observables by applying a double differencing technique to eliminate phase biases related to drifts in the satellite and receiver clock oscillators. GPS phase data were weighted according to an elevation-angle-dependent error model¹⁰ using an iterative analysis procedure whereby the elevation dependence was determined by the observed scatter of phase residuals. In this analysis the parameters of satellites orbit were fixed to the IGS final products. IGS absolute antenna phase center models (igs08.atx and igs14_www.atx available at <ftp://ftp.igs.org/pub/station/general/>; see also Table 2) for both satellite and ground-based antennas were adopted in order to improve the accuracy of vertical site position component estimations^{15,16}. The first-order ionospheric delay was eliminated by using the ionosphere-free linear combination, while a second-order ionospheric corrections¹⁷ were applied using the IONEX files from the Center for Orbit Determination in Europe (CODE). The tropospheric delay was modeled as a piecewise linear model and estimated using the Vienna Mapping Function 1 (VMF1¹⁸) with a 10° cutoff. The Earth Orientation Parameters (EOP) were tightly constrained to priori values obtained from IERS Bulletin B. The ocean tidal loading was corrected using the FES2004¹⁹ model. The International Earth Rotation Service (IERS) 2003 model for diurnal and semidiurnal solid Earth tides was also adopted.

In a successive step, the GAMIT solutions, in the form of loosely-constrained H-files, were aligned to the IGB08 reference frame. Such an alignment was performed by INGV-CT and DICAM-UniBO through the GLOBK/GLORG¹⁰ software package by minimizing the deviations between horizontal positions and velocities of achieved solutions and those available in the IGB08.snrx²⁰ reference solutions (Table 2). INGV-BO, instead, performed the alignment to the IGB08 reference frame through the ST_FILTER program of the QOCA^{21,22} software and by combining all the daily loosely constrained solutions with the global solution of the IGS network made available by MIT (ftp://everest.mit.edu/pub/MIT_GLL/), and simultaneously realizing a global reference frame

by applying generalized constraints²¹. Specifically, the reference frame was defined by minimizing the velocities of the IGS core²³ stations, while estimating a seven-parameter transformation with respect to the GNSS realization of the ITRF2008⁶ frame, i.e., the IGB08³ reference frame.

Raw data processing by using the GIPSY software. GIPSY is a GNSS-Inferred Positioning System and Orbit Analysis Simulation software package (<https://gipsy-oasis.jpl.nasa.gov/>) developed by the Jet Propulsion Laboratory. Data processing with this software package was performed at DICAM-UniBO (which used GIPSYX, version rc0.4) and INGV-ONT (which used GIPSY-OASIS II, version 6.3).

Raw observations were processed by both analysis centers in a precise point positioning mode applied to ionospheric-free carrier phase and pseudorange data²⁴ and using JPL's final fiducial-free GNSS orbit products. Ocean loading tidal loading and companion tides, computed using the FES2004¹⁹ tidal model coefficients (<http://holt.oso.chalmers.se/loading>) and were applied as a station motion model. The wet zenith troposphere and two gradient parameters were estimated every 5 minutes as a random walk process²⁵ by using the VMF1¹⁸ with a 10° cutoff. A second-order ionospheric correction²⁶ was applied during the data processing. Station clock errors were treated as a white-noise process. The ambiguity resolution was performed by using the wide lane and phase bias (WLPB) method²⁴, which phase-connects individual stations to IGS stations in common view. Resolving ambiguities reduced significantly the scatter mostly in the east component of time series. Satellite orbits and clock parameters were provided by JPL who determine them in a global fiducial free analysis using a subset of the available IGS core stations as tracking sites.

In this step, the *ONT_GIPSY* solution was aligned to IGS14⁴ by applying a daily seven-parameter Helmert transformation (three rotations, three translations, and a scale component obtained from JPL) specifically calculated using the IGS14 Cartesian coordinates and velocities of 132 stations selected by specific quality criteria (e.g. long observation time, continuity through time, position and velocity constrained with sub-millimeter level accuracy, etc.) and located in and around the Eurasian plate and in the Mediterranean area²⁷. This reference frame realization method applies a continental-scale spatial filter to the station coordinates, leading to a reduction of the common-mode errors²⁸ and to an increase of the signal-to-noise ratio.

The *UBO_GIPSY* solution was aligned to the IGB08³ reference frame by applying a daily seven-parameter Helmert transformation which was ad hoc calculated using as reference a regional subset of IGS tracking network (see Table 2). The reference coordinates of this regional subset can be found in the IGB08.sn²⁰ file provided by IGS.

Each analysis center, in the end, provided position time-series in a common format (e.g. the UNAVCO PBO “pos” ASCII file format⁷); the *ONT_GIPSY* solution was aligned to IGS14 while the other solutions were aligned to IGB08. It must be noted that some few stations show time series with different temporal length because each analysis center requested the RINEX dataset to Eni S.p.A. at different times. Moreover, the *ONT_GIPSY* solution spans the 2000.0–2017.99 time interval since the limited number of continuous stations doesn't allow to adequately constraint the adopted continental-scale spatial filter prior to 2000.

Data Records

All the computed raw time series are distributed via the PANGEA repository²⁹ so that the interested researchers can use them for future studies. The raw time series (in ASCII pos format) were stored in different folders and accordingly renamed, based on the solutions described in paragraph “Raw data processing”.

We included in the same repository:²⁹

- A file, named “ENI_Offsets.json”, containing all manually picked offsets; as mentioned above it can be used as input for later use in the TSAAnalyzer software²⁴.
- All logs files as resulting from the analysis performed with the TSAAnalyzer software; the logs files were renamed accordingly to the associated solution. These logs contain all the parameters discussed in section 3.
- The phasor diagrams in png format.
- The time series plots (observed, modelled and residual components) in png format; the plots were renamed accordingly to the associated solution.
- The time series comparison plots in png format.

The original raw RINEX data are property of Eni S.p.A. company. Interested users can obtain free access to data under a specific confidential agreement by contacting Eni S.p.A. company (see the Supplementary Information for details).

Technical Validation

As mentioned above, the position time series computed by each analysis center as well as the estimated velocity fields were compared in order to highlight possible differences arising from the use of the different software and from the specific models that were selected and applied in the analysis.

Position time series comparison. To perform a simple comparison between the position time series computed by each analysis center we used the TSAAnalyzer^{30,31} open-source software which reads GNSS position time series with different formats and allows to remove outliers as well as to simultaneously estimate linear and seasonal signals.

Roughly speaking, position time series can be modelled as the superposition of three main types of signals: (i) linear long-term deformation, (ii) seasonal signals, (iii) instrumental (e.g., GNSS antenna changes) and tectonic (co-seismic displacement) offsets. Therefore, site motion $y(t)$ for each component can be modelled as:

| Site | Offset date | Notes |
|------|-------------|-----------|
| AMEB | 26/10/2011 | unknown |
| | 15/03/2012 | unknown |
| | 20/03/2012 | unknown |
| | 01/04/2012 | unknown |
| | 07/04/2012 | unknown |
| | 11/04/2012 | unknown |
| | 12/05/2012 | unknown |
| | 17/05/2012 | unknown |
| | 04/12/2012 | equipment |
| ELEO | 30/10/2016 | tectonic |
| EMIL | 29/07/2015 | unknown |
| | 25/01/2016 | unknown |
| FALC | 30/10/2016 | tectonic |
| GARC | 06/10/2011 | unknown |
| GRTM | 22/06/2010 | unknown |
| | 24/08/2016 | tectonic |
| | 30/10/2016 | tectonic |
| | 14/12/2017 | unknown |
| ITGS | 24/08/2016 | tectonic |
| | 30/10/2016 | tectonic |
| NAPA | 01/01/2012 | unknown |
| PCWC | 07/10/2009 | unknown |
| | 14/07/2011 | unknown |
| PINE | 24/08/2016 | tectonic |
| | 30/10/2016 | tectonic |
| SMAR | 31/08/2011 | unknown |

Table 3. Offsets manually picked and recorded in the “ENI_Offsets.json” file which is available on the repository.

$$y(t_i) = a + bt_i + c \sin(2\pi t_i) + d \cos(2\pi t_i) + e \sin(4\pi t_i) + f \cos(4\pi t_i) + \sum_{j=1}^{n_g} g_j H(t_i - T_{g_j}) + v_i \quad (1)$$

where t_i for $i = 1 \dots N$ are the daily solution epochs (in units of years). The terms a and b are the site position and the linear rate; coefficients c and d describe the annual periodic motion while e and f stand for the semi-annual motion. The summation term corrects for any number (n_g) of offsets, with magnitudes g and epoch T_g using the Heaviside³² step function H and the last term, v_i , is the residual.

A first visual inspection of all raw coordinates time series reveals that they contain both offsets and outliers. Outliers showing large uncertainties (e.g. blunders) were removed by setting in TSAAnalyzer an arbitrary sigma criterion (we set 15, 15 and 20 mm, for North, East and Up components, respectively). Offsets were manually picked and recorded in the “ENI_Offsets.json” file (available on the repository) for later use (see also Table 3). Offsets classified as “tectonic” correspond to co-seismic deformation related to the $M > 6$ earthquakes striking central Italy on 24 August 2016 and on 26 October 2016³³. Offsets classified as “equipment” correspond to change in antennas while offsets classified as “unknown” are characterized by suspicious motion whose nature should be related to service operations on platform.

Finally, estimated parameters for each solution are reported as ASCII log files in the online repository. The following analysis is based on the results achieved with this time-series analysis.

The Weighted Root Mean Squares (WRMS) values of all time-series were also estimated by using the TSAAnalyzer software (see log files on the repository), after filtering outliers and estimating parameters according to Eq. (1). In such a step, each single daily solution was weighted with respect to its formal sigma without taking into account the correlation between the North, East and Up components. Frequency histograms of WRMS values for horizontal and vertical components of each different solution analyzed in this study are reported in Fig. 2, while range, mean and median values are reported in Table 4. All solutions are characterized by very similar values, highlighting similar patterns between the solutions as for instance, (i) the mean and median WRMS values for vertical component are about three times larger than the horizontal ones and (ii) the higher WRMS values are observed always at the same stations (CERA and AMEB; see the related logs file in the repository for additional details). Moreover, computed WRMS values are in the same range of the ones estimated for on-shore stations with comparable observing time windows^{13,34}.

All the examined time series contain significant seasonal signals in both horizontal and vertical directions. Values estimated for each solution show a large agreement between them; annual amplitudes range between 0.5–5.3 mm horizontally and 3–8 mm vertically with higher values observed at sites installed on the offshore

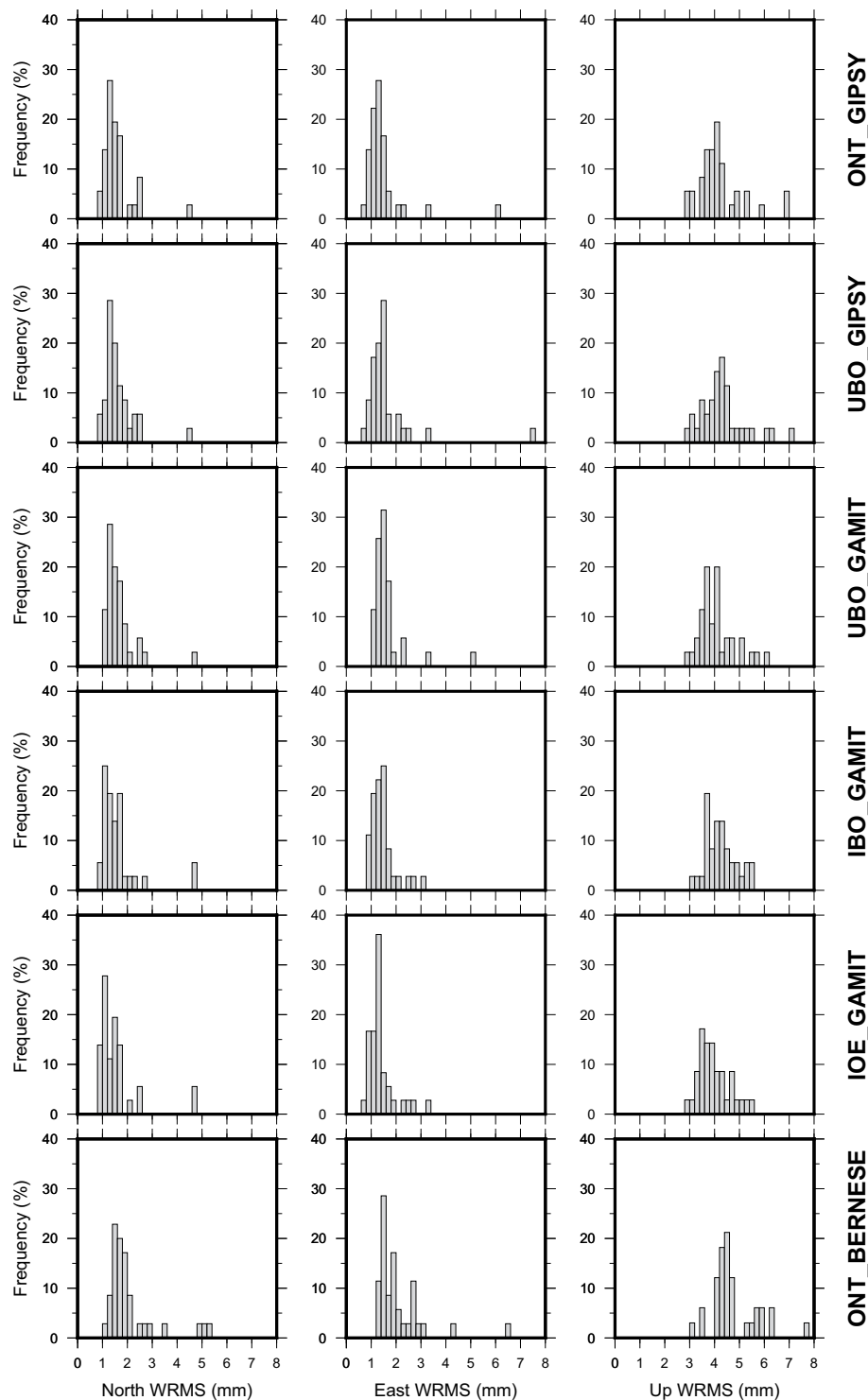


Fig. 2 Frequency histograms of WRMS values for the North, East and Up components of filtered residual time series.

platforms (see plots reported in the online repository). Semi-annual amplitudes are usually <0.5 mm horizontally and ~ 1 mm vertically. Additional features on seasonal signals are provided by considering phasor diagrams of amplitudes and phase signals (see the example reported in Fig. 3). Regarding the annual signals, most of the sites installed on the offshore platforms show maximum amplitudes on January, September and August for North, East and Up components, respectively. Moreover, most of these sites (especially those closely located to the coastal area) are subjected to horizontal oscillations with a prevailing NNW-SSE attitude and to vertical oscillation associated with uplift during summer and subsidence during winter. Sites installed along the coastal

| Solution | North | | | East | | | Up | | |
|-------------|-----------|------|--------|-----------|------|--------|-----------|------|--------|
| | Range | Mean | Median | Range | Mean | Median | Range | Mean | Median |
| IBO_GAMIT | 0.94–4.79 | 1.64 | 1.40 | 0.93–3.17 | 1.49 | 1.39 | 3.06–8.01 | 4.37 | 4.20 |
| IOE_GAMIT | 0.88–4.96 | 1.55 | 1.28 | 0.75–3.26 | 1.39 | 1.28 | 2.85–8.67 | 4.12 | 3.87 |
| ONT_BERNESE | 1.02–5.21 | 2.09 | 1.73 | 1.21–6.43 | 2.08 | 1.84 | 3.18–9.40 | 5.00 | 4.55 |
| ONT_GIPSY | 0.89–4.43 | 1.58 | 1.42 | 0.70–6.05 | 1.48 | 1.27 | 2.95–6.95 | 4.21 | 4.05 |
| UBO_GAMIT | 1.08–4.63 | 1.66 | 1.44 | 1.04–5.18 | 1.65 | 1.49 | 2.91–6.08 | 4.08 | 3.97 |
| UBO_GIPSY | 0.94–4.54 | 1.64 | 1.49 | 0.80–7.49 | 1.63 | 1.41 | 2.96–7.06 | 4.33 | 4.27 |

Table 4. Range, mean and median values (in mm) for time series residuals WRMS.

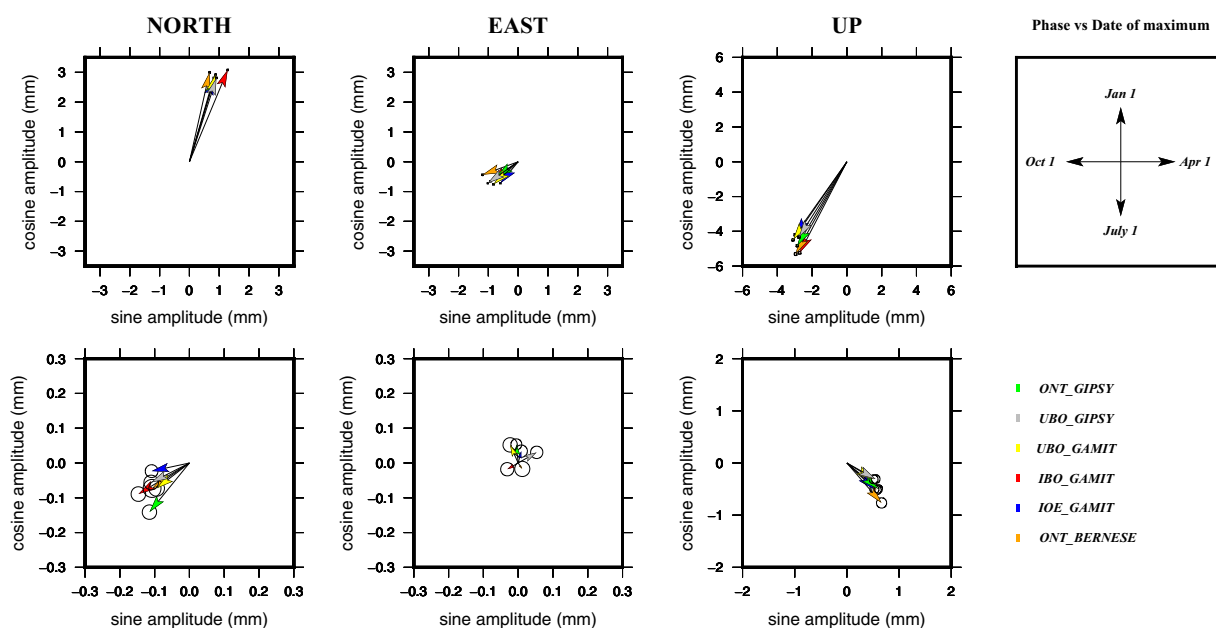


Fig. 3 Example of phasor diagrams of annual (top) and semiannual (bottom) signals for station AGOB (see Table 1). Amplitudes of the estimated sine and cosine parameters (see Eq. (1)) are plotted for the North, East and Up components. The upper-right plot represents the key to correlate the maxima phase direction with the day year period. Phases are referred to January 1 and time increases clockwise.

area are characterized by maximum amplitudes largely scattered and no clear oscillation patterns can be recognized. Concerning the semiannual signals, most of the sites show maximum amplitudes concentrated during July–September for North component and during April–June for both East and Up components.

Some position time series (mainly recorded at the stations located on the offshore platforms) exhibit a curved shape, while others show weak post-seismic decay (recorded at few stations located along the coastal area, eastward of the 2016 seismic sequence epicentral area). Both features result in deviations from the linear trend; to quantify such a deviation for each time series, we defined a simple non-linearity index (I_{NL}) as the ratio between the standard deviation of the smoothed time series and the standard deviation of its intrinsic noise:

$$I_{NL} = \frac{\sqrt{\sum_{i=1}^N |F_i - \bar{F}|}}{\sqrt{\sum_{i=1}^N |R_i - \bar{R}|}} \quad (2)$$

where $i = 1 \dots N$ is the number of data, F and R (with mean values \bar{F} and \bar{R}) are the smoothed and the residual observations. The smoothed time series should approximate the low frequency non-linear behavior, while the residual time series (computed as the difference between the unsmoothed and the smoothed time series) would contain most of the high frequency noise and should be regarded as a good indicator of the station intrinsic noise. Therefore, by taking into account the time series already de-trended with respect to Eq. (1), we computed i) the smoothed time series by applying a moving average filter with a time span of 1 year, ii) the related residual time series and finally, iii) the I_{NL} values (Table 5). Estimations of I_{NL} index on a set of high-quality IGS stations (Table 2) highlight that values < 0.5 reflect time series with pure linear behavior, therefore in the following we arbitrarily set as “gentle” and “moderately” non-linear all the time series with $0.5 \leq I_{NL} \leq 1$ and $I_{NL} > 1$, respectively (Table 5). Based on this simple definition and excluding FRAT station because of its short time series, 11

| Site | North | East | Up |
|------|-------------|-------------|-------------|
| AGOB | 0.61 ± 0.08 | 0.41 ± 0.09 | 0.74 ± 0.07 |
| AMEB | 0.19 ± 0.08 | 0.55 ± 0.22 | 0.45 ± 0.18 |
| ANBL | 0.71 ± 0.11 | 0.61 ± 0.13 | 0.90 ± 0.12 |
| ANEB | 0.97 ± 0.25 | 0.34 ± 0.10 | 0.36 ± 0.14 |
| ANGA | 1.04 ± 0.39 | 1.09 ± 0.40 | 1.61 ± 0.69 |
| ANLS | 0.30 ± 0.05 | 0.51 ± 0.20 | 0.66 ± 0.21 |
| ANTA | 0.54 ± 0.06 | 0.76 ± 0.12 | 0.79 ± 0.17 |
| ANTO | 0.46 ± 0.06 | 0.39 ± 0.07 | 0.33 ± 0.08 |
| ARIA | 1.15 ± 0.13 | 0.35 ± 0.10 | 0.70 ± 0.10 |
| ARMI | 0.40 ± 0.05 | 0.53 ± 0.08 | 0.40 ± 0.05 |
| AZAB | 0.34 ± 0.07 | 0.33 ± 0.10 | 0.49 ± 0.06 |
| BRIS | 0.48 ± 0.19 | 0.39 ± 0.14 | 0.28 ± 0.04 |
| CERA | 2.48 ± 1.09 | 0.72 ± 0.47 | 0.50 ± 0.26 |
| CLAE | 1.82 ± 0.11 | 1.30 ± 0.28 | 0.37 ± 0.03 |
| CROT | 0.98 ± 0.23 | 0.47 ± 0.15 | 0.51 ± 0.05 |
| ELEO | 0.32 ± 0.08 | 0.24 ± 0.07 | 0.17 ± 0.05 |
| EMIL | 0.30 ± 0.09 | 0.34 ± 0.05 | 0.28 ± 0.04 |
| FALC | 0.36 ± 0.05 | 0.29 ± 0.03 | 0.26 ± 0.05 |
| FANO | 0.54 ± 0.03 | 0.48 ± 0.10 | 0.28 ± 0.10 |
| FAUZ | 0.10 ± 0.03 | 0.24 ± 0.05 | 0.32 ± 0.03 |
| FIUN | 1.44 ± 0.26 | 3.11 ± 1.11 | 1.26 ± 0.09 |
| FRAT | 0.02 ± 0.00 | 0.01 ± 0.00 | 0.01 ± 0.00 |
| GARB | 0.59 ± 0.14 | 0.71 ± 0.18 | 0.82 ± 0.07 |
| GARC | 0.58 ± 0.33 | 0.52 ± 0.42 | 0.67 ± 0.33 |
| GRTM | 0.21 ± 0.05 | 0.23 ± 0.03 | 0.17 ± 0.04 |
| ITGS | 0.77 ± 0.10 | 0.82 ± 0.10 | 0.33 ± 0.06 |
| MANA | 0.52 ± 0.09 | 0.55 ± 0.13 | 0.26 ± 0.04 |
| NAID | 0.40 ± 0.09 | 0.45 ± 0.06 | 0.53 ± 0.05 |
| NAPA | 0.40 ± 0.11 | 0.72 ± 0.14 | 0.29 ± 0.07 |
| PCCP | 0.42 ± 0.07 | 0.46 ± 0.13 | 0.40 ± 0.08 |
| PCTA | 1.16 ± 0.19 | 1.08 ± 0.30 | 0.79 ± 0.12 |
| PCWC | 0.36 ± 0.11 | 0.34 ± 0.07 | 0.77 ± 0.23 |
| PINE | 0.28 ± 0.04 | 0.23 ± 0.05 | 0.22 ± 0.04 |
| RUBI | 0.48 ± 0.05 | 0.54 ± 0.06 | 0.69 ± 0.07 |
| SMAR | 0.28 ± 0.07 | 0.45 ± 0.09 | 0.60 ± 0.08 |
| TEAL | 1.14 ± 0.09 | 1.10 ± 0.19 | 0.71 ± 0.13 |
| TREV | 0.26 ± 0.07 | 0.29 ± 0.07 | 0.23 ± 0.06 |

Table 5. Mean I_{NL} index values and associated standard deviation (based on the values computed for all the different time series solutions) for North, East and Up components.

stations are generally characterized by linear time series (for all the three components) while the other are characterized by gentle (19 stations) and moderately (6 stations) non-linear time series, at one or more components. Stations with gentle and moderately non-linear time series mainly concentrates offshore on northern Adriatic Sea and onshore, along the coastal belt; the stations with linear time series are mainly located along the coastal onshore belt.

As a last step, the time-series were compared between them after correcting the offsets (Table 3) and removing the linear trend as defined in Eq. (1). An example of such a comparison is reported in Fig. 4, while the remaining plots are reported in the online repository. This simple comparison highlights how the main features characterizing the time-series (e.g. seasonal signals, noisier time intervals, short-term transients, etc.) show a good agreement between the different solutions.

Velocity field analysis and comparison. In the following, we performed some simple comparisons between all the computed linear trend values; however, these analyses (and related results) must be considered with caution because of the non-linear motion detected at many stations.

As a first step, we calculated the residual values with respect to the mean ones for each solution and for each component (Table 6). Results are reported as frequency histograms in Fig. 5. Regarding the North component, the IBO_GAMIT, the IOE_GAMIT and the ONT_GIPSY solutions show values up to 0.2 mm smaller than the mean values, while the ONT_BERNESE solution shows values up to 0.4 mm larger than the mean values; the

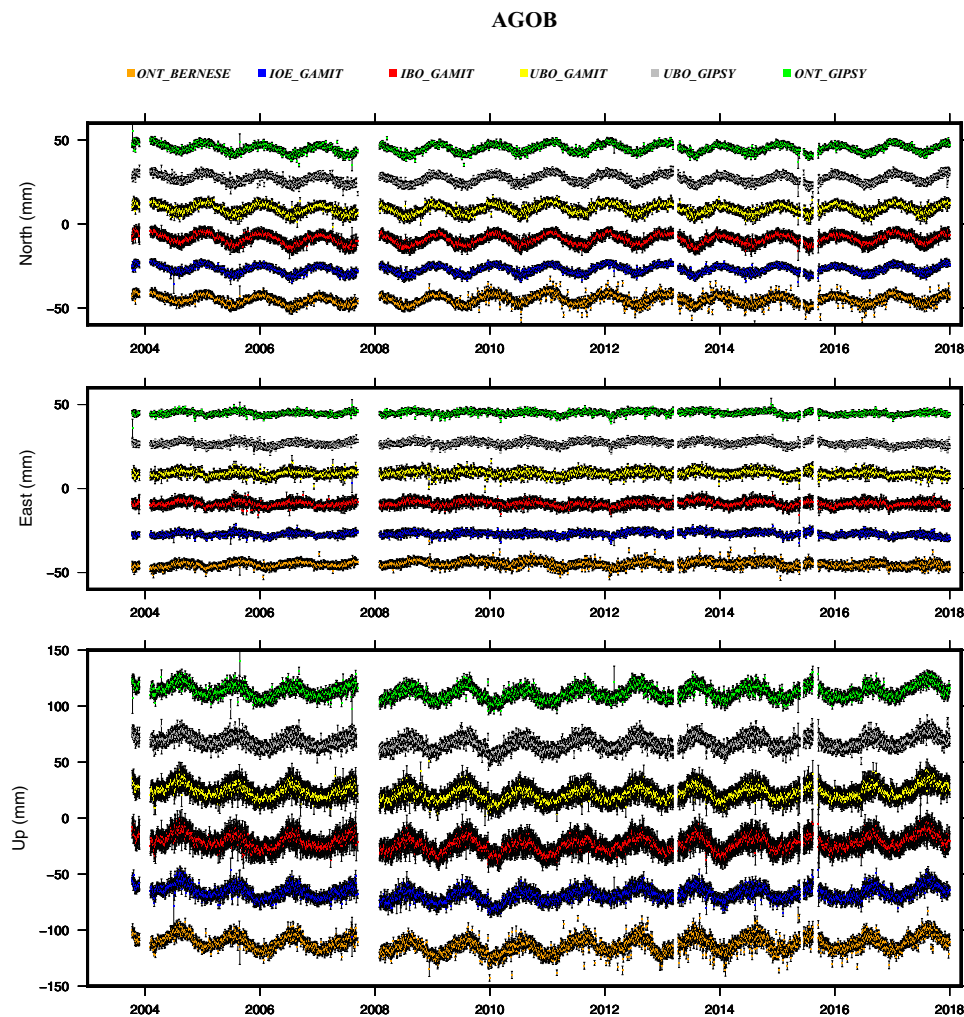


Fig. 4 Example of time series comparison from the different solution described in the main text. Each time series is reported after correcting offsets and removing the linear trend as defined in Eq. (1).

UBO_GAMIT and UBO_GIPSY solutions show values centered (± 0.1 mm) on the mean values. Regarding the East component, the IBO_GAMIT, the IOE_GAMIT and the ONT_BERNESE solutions show values up to 0.2 mm larger than the mean values, while the ONT_GIPSY solution shows values up to 0.4 mm smaller than the mean values; the UBO_GAMIT and UBO_GIPSY show again values centered (± 0.1 mm) on the mean values. Regarding the Up component, the IBO_GAMIT, the IOE_GAMIT, the UBO_GAMIT and the UBO_GIPSY solutions show prevailing values up to 0.6 mm larger than the mean values, while the ONT_GIPSY and the ONT_BERNESE solutions show prevailing values up to 0.4 mm smaller than the mean values; the overall differences range in the -0.6 to 0.6 mm value interval.

As a second step, we computed for each solution the velocity field with respect to a Eurasian³⁵ reference frame; achieved results are reported in Fig. 6. Because of its simple definition, such a rotation affects only the horizontal velocities; therefore, the vertical ones remained constrained in their previous reference frame. Considering the horizontal velocity (Fig. 6), all the solutions show a general agreement in terms of azimuthal pattern and vector magnitudes, however the ONT_BERNESE solution show a systematic counterclockwise rotation with respect to the other ones, probably related to the Helmert constraints imposed for the reference frame transformation (Table 2). The ONT_GIPSY solution, although referred to IGS14, is highly coherent with the other solutions. Most of the stations installed along the onshore coastal area show a prevailing NNW-oriented velocity pattern which is highly coherent with the regional deformation field^{14,27,36}. Stations installed along the Adriatic offshore show a complex deformation field characterized by large variations both in the azimuthal pattern and the vector magnitudes (Fig. 6).

The vertical velocities are reported in Fig. 7 as averaged values (panel a) and as differences with respect to the average values (panel b). Figure 7a shows that most of the stations installed along the onshore coastal area are characterized by subsidence with rates up to 2 mm/yr in agreement with recent studies⁸, while all the stations installed on the offshore platforms exhibit a general subsidence with rates up to ~ 17 mm/yr (see also Table 6). The site-by-site comparisons reported in Fig. 7b confirm the features previously recognized: the ONT_GIPSY and ONT_BERNESE solutions are generally smaller than the mean values, while the other solutions are larger than

| Site | North | East | Up |
|------|--------------|--------------|---------------|
| AGOB | 16.77 ± 0.19 | 22.62 ± 0.12 | -7.14 ± 0.42 |
| AMEB | 17.38 ± 0.24 | 20.52 ± 0.18 | -3.07 ± 0.41 |
| ANBL | 18.32 ± 0.16 | 21.96 ± 0.15 | -3.74 ± 0.38 |
| ANEB | 17.79 ± 0.06 | 20.98 ± 0.18 | -4.80 ± 0.40 |
| ANGA | 19.41 ± 0.22 | 22.16 ± 0.14 | -17.56 ± 0.52 |
| ANLS | 18.12 ± 0.17 | 21.18 ± 0.18 | -4.23 ± 0.34 |
| ANTA | 18.14 ± 0.19 | 20.74 ± 0.16 | -4.91 ± 0.35 |
| ANTO | 18.45 ± 0.16 | 21.34 ± 0.16 | -2.26 ± 0.41 |
| ARIA | 17.84 ± 0.20 | 23.18 ± 0.18 | -10.79 ± 0.56 |
| ARMI | 17.75 ± 0.13 | 21.94 ± 0.16 | -4.39 ± 0.41 |
| AZAB | 18.65 ± 0.18 | 22.18 ± 0.15 | -3.64 ± 0.39 |
| BRIS | 18.96 ± 0.17 | 23.09 ± 0.16 | 1.55 ± 0.39 |
| CERA | 18.32 ± 0.19 | 22.74 ± 0.13 | -11.66 ± 0.36 |
| CLAE | 15.73 ± 0.15 | 21.25 ± 0.15 | -14.31 ± 0.37 |
| CROT | 17.73 ± 0.18 | 27.24 ± 0.10 | -0.24 ± 0.60 |
| ELEO | 17.98 ± 0.16 | 23.11 ± 0.10 | 0.08 ± 0.52 |
| EMIL | 18.23 ± 0.10 | 23.13 ± 0.21 | -1.89 ± 0.31 |
| FALC | 18.46 ± 0.13 | 23.00 ± 0.17 | -0.15 ± 0.38 |
| FANO | 18.91 ± 0.14 | 22.40 ± 0.16 | 0.15 ± 0.38 |
| FAUZ | 19.77 ± 0.20 | 20.55 ± 0.26 | -5.65 ± 0.47 |
| FIUN | 15.56 ± 0.19 | 28.72 ± 0.09 | -14.18 ± 0.43 |
| GARB | 17.77 ± 0.18 | 20.98 ± 0.14 | -7.06 ± 0.42 |
| GARC | 17.15 ± 0.08 | 19.73 ± 0.08 | -8.56 ± 0.28 |
| GRTM | 18.50 ± 0.10 | 23.68 ± 0.15 | -0.30 ± 0.30 |
| ITGS | 19.07 ± 0.09 | 22.70 ± 0.14 | 0.13 ± 0.36 |
| MANA | 17.33 ± 0.17 | 21.59 ± 0.14 | -2.98 ± 0.46 |
| NAID | 17.82 ± 0.17 | 20.51 ± 0.15 | -3.53 ± 0.42 |
| NAPA | 17.56 ± 0.20 | 21.45 ± 0.08 | -1.52 ± 0.34 |
| PCCP | 16.84 ± 0.18 | 23.29 ± 0.15 | -4.14 ± 0.38 |
| PCTA | 19.65 ± 0.18 | 23.86 ± 0.11 | -7.57 ± 0.40 |
| PCWC | 17.01 ± 0.21 | 22.11 ± 0.04 | -5.30 ± 0.51 |
| PINE | 18.64 ± 0.10 | 23.18 ± 0.18 | -0.74 ± 0.35 |
| RUBI | 19.39 ± 0.13 | 22.13 ± 0.16 | -2.28 ± 0.36 |
| SMAR | 18.39 ± 0.21 | 20.94 ± 0.05 | -6.54 ± 0.47 |
| TEAL | 18.21 ± 0.16 | 19.76 ± 0.16 | -4.55 ± 0.39 |
| TREV | 17.23 ± 0.16 | 20.51 ± 0.15 | -0.10 ± 0.44 |

Table 6. Mean linear rate values and associated standard deviation (in mm) for North, East and Up components. No estimates were performed for the FRAT site because of its short time series.

the mean values. These differences seem related to the adopted reference (the ONT_GIPSY solution is referred to IGS14) and/or to the constraints imposed for the reference frame transformation (the ONT_BERNESE solution adopts a Helmert transformation based only on 4-parameters).

Final considerations. As mentioned above, computed position time series were analyzed by means of the TSAlyzer^{30,31} open-source software in order to estimate the linear and seasonal components as well as the offsets values.

We detected some offsets corresponding to equipment changes and to co-seismic deformation. Moreover, some detected offsets, classified as “unknown” in Table 3, are characterized by motion probably related to service operations on platform. All detected offsets have been identified in all solutions and are characterized by very similar values (see related log files on the online repository).

Examined position time series contain significant seasonal signals: annual amplitudes range between 0.5–5.3 mm horizontally and 3–8 mm vertically while semi-annual amplitudes are usually < 0.5 mm horizontally and ~1 mm vertically. Higher annual amplitude values were observed only at sites installed on the offshore platforms, with maximum amplitudes on January, September and August for North, East and Up components, respectively. The horizontal oscillations occur with a prevailing NNW-SSE attitude while the vertical oscillation are associated with uplift during summer and subsidence during winter. Conversely, sites installed along the coastal area are characterized by maximum amplitudes largely scattered and no clear oscillation patterns can be recognized. All these observations suggest that offshore stations would be affected by variations in hydrostatic pressure and

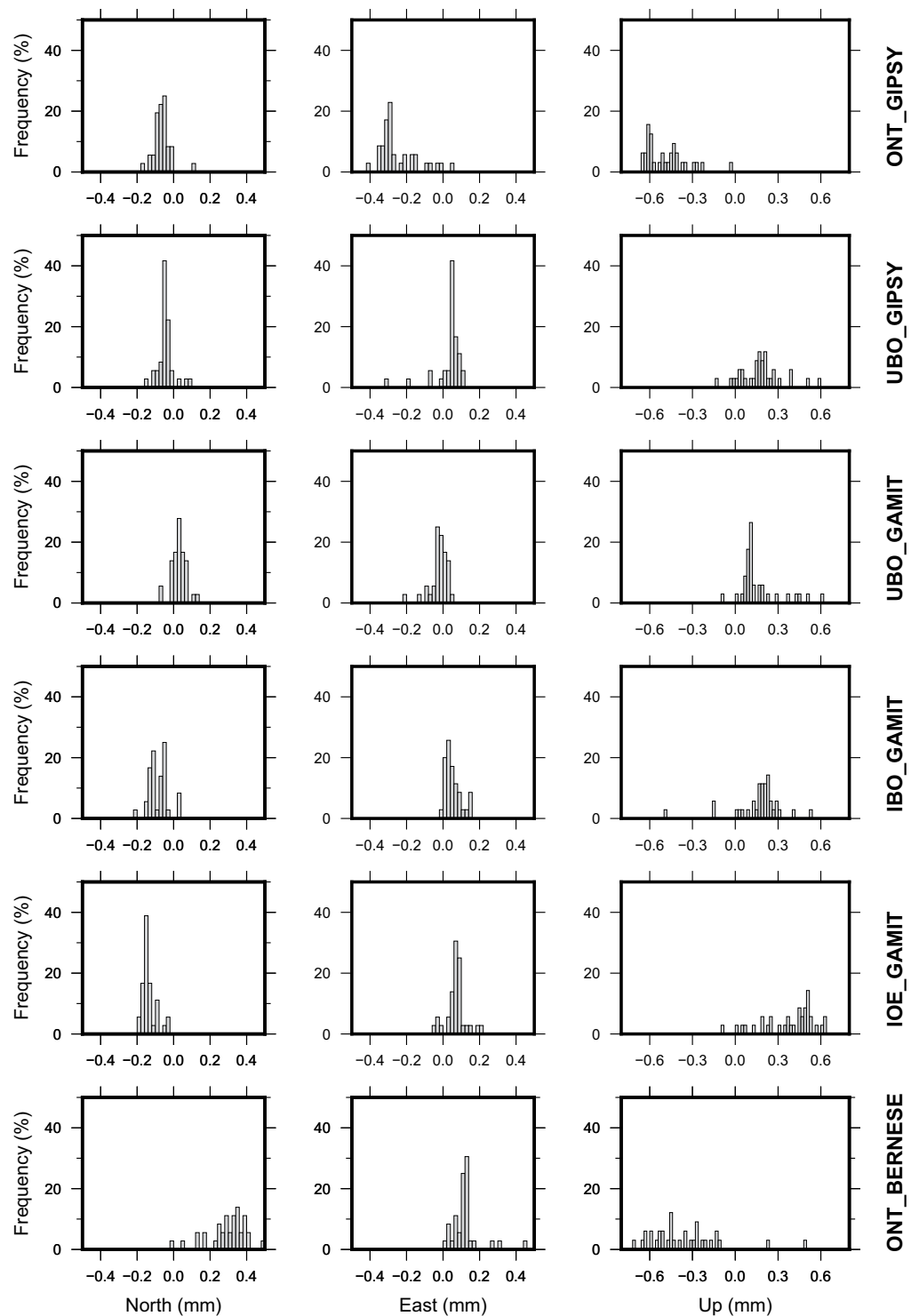


Fig. 5 Frequency histograms of residual values between computed linear trend values with respect to the mean values (Table 5).

buoyancy on tubular members of the platforms caused by changes in tide levels. Moreover, since the Adriatic Sea is an almost land-locked basin where atmospheric conditions and vary considerably with the seasons^{37,38}, environmental loads caused by wind (e.g. periodic seiche-like effects), current flows and waves would substantially contribute to the observed seasonal oscillations. Due to the main metallic-fabric of platform, seasonal thermal expansion-contraction cycles of the tiny structures could also contribute to the seasonal oscillations.

A large number of stations is characterized also by position time series with non-linear behavior at one or more components, as quantified by the computed I_{NL} index (Table 5). Stations with I_{NL} values larger than 1

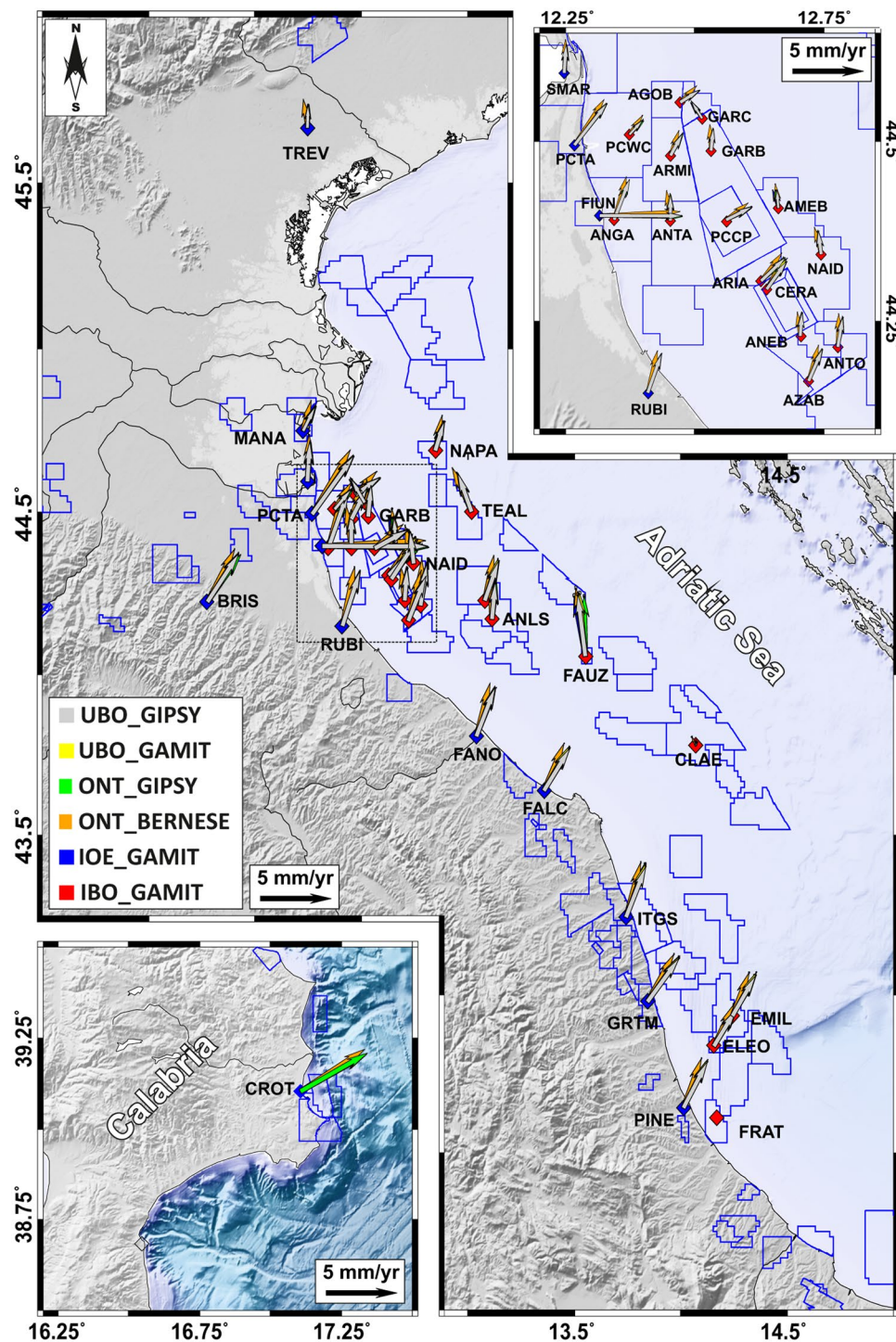


Fig. 6 Horizontal velocity field comparisons. Velocities are referred to a Eurasian³⁵ reference frame. Lower inset: zoom on Calabria region; upper inset: zoom on the Northern Adriatic region.

are generally characterized also by high subsidence rates (Table 6 and Fig. 7), clearly suggesting that, the tectonic deformation is superseded by the local sources ones (e.g. reservoir depletion, sediment compaction, etc.). Moreover, these local sources affected also the horizontal deformation rates leading to a complex pattern, strictly depending by the relative position of the station (i.e. the platform) with respect to the sources of deformation. Similar considerations can be done for the stations with $0.5 \leq I_{NL} \leq 1$, where however, the effects of local sources have had a minor influence on station motion. Conversely, stations with $I_{NL} < 0.5$ show a velocity pattern which is highly coherent with the regional deformation field of the investigated area.

Based on the analysis and the comparisons performed in this study, the different time series solutions are highly consistent between them despite the use of different software, models, strategy processing and frame

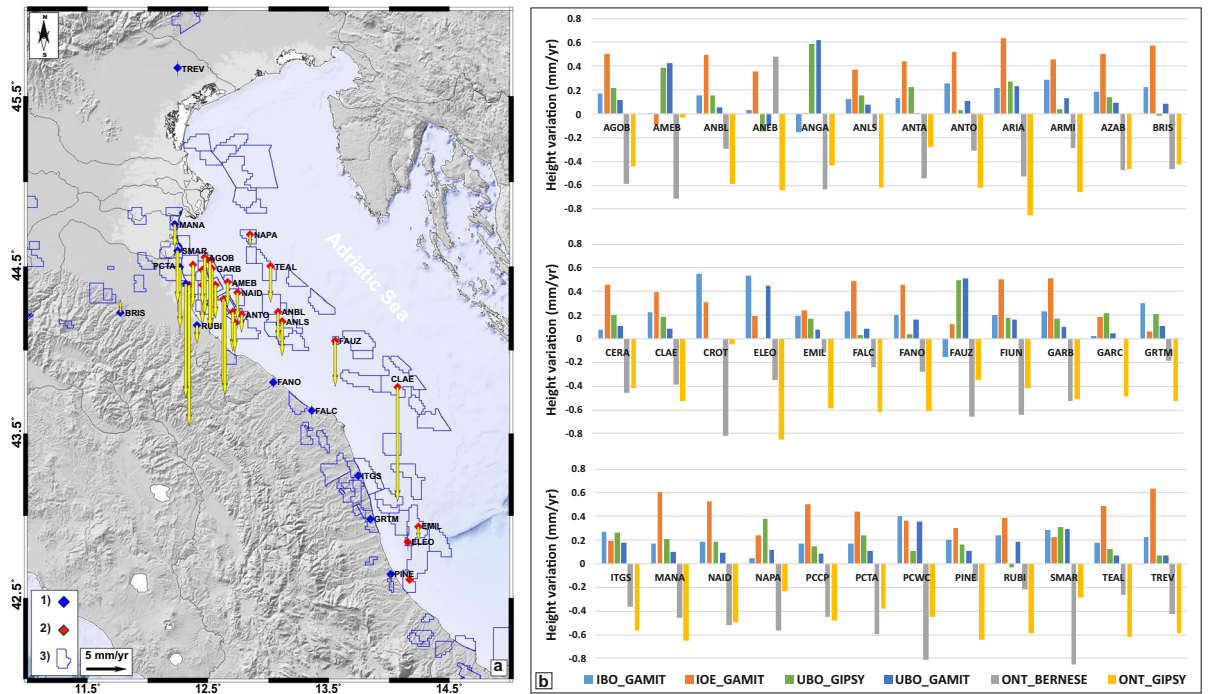


Fig. 7 (a) mean vertical velocity field 5; (b) comparison of the residual vertical velocity values for all the analyzed solutions.

realizations. The analyzed dataset represents an invaluable dataset since it allows to improve the current GNSS stations density along the Adriatic coastal belt. In addition, this dataset allowed to discover a complex interplay between regional and local sources of deformation, whose relationships would be addressed in future analysis. Indeed, because of their uniqueness, these data could improve and promote further studies in offshore exploiting contexts including: (i) measurement and modelling of induced subsidence patterns and their spatial and temporal correlation with production data, (ii) estimation of natural and anthropic contributions to the overall ground subsidence, (iii) improvement on the long-term regional crustal deformation on offshore areas, (iv) coast-line dynamic and impact on human activities and natural ecosystems (e.g. coast line setback).

Received: 7 April 2020; Accepted: 1 October 2020;

Published online: 04 November 2020

References

- Antonucci, I. *et al.* Multidisciplinary study on assessment of subsurface deformations caused by offshore hydrocarbon activity in Emilia Romagna region, aimed to develop a methodological approach for an integrated monitoring. In *Proceedings of 37th GNSS*, <http://www3.inogs.it/gngts/files/2018/S23/Riassunti/Antonucci.pdf> (2018).
- Haines, B. J., Desai, S. D. & Born, G. H. GPS monitoring of vertical seafloor motion at Platform Harvest. *Advan. Space Res.* **51**, 1369–1382 (2013).
- Reibischung, P. [IGSMail-6663] IGB08: an update on IGS08 <https://lists.igs.org/pipermail/igsmail/2012/000497.html> (2012).
- Reibischung, P., Altamimi, Z., Ray, J. & Garayt, B. The IGS contribution to ITRF2014. *J. Geod.* **90**, 611–630 (2016).
- Altamimi, Z., Reibischung, P., Métivier, L. & Collilieux, X. ITRF2014: A new release of the International Terrestrial Reference Frame modeling nonlinear station motions. *J. Geophys. Res.* **121**, 6109–6131 (2016).
- Altamimi, Z., Collilieux, X. & Métivier, L. ITRF2008: an improved solution of the international terrestrial reference frame. *J. Geodesy* **85**(8), 457–473 (2011).
- UNAVCO. Notice to UNAVCO GPS data product users: file format update <https://www.unavco.org/data/gps-gnss/derived-products/docs/NOTICE-TO-DATA-PRODUCT-USERS-GPS-2013-03-15.pdf> (2013).
- Dach, R., Lutz, S., Walser, P. & Fridez, P. Bernese GNSS Software Version 5.2. *Astronomical Institute, University of Bern* <http://www.berne.unibe.ch/docs/DOC52.pdf> (2015).
- Dach, R., Hugentobler, U., Fridez, P. & Meindl, M. Bernese GNSS Software, Version 5.0. *Astronomical Institute, University of Bern* <http://www.berne.unibe.ch/docs/DOC50.pdf> (2007).
- Herring, T. A., King, R. W., Floyd, M. A. & McClusky, S. C. Introduction to GAMIT/GLOBK, Release 10.7. *Massachusetts Institute of Technology* http://geoweb.mit.edu/gg/Intro_GG.pdf (2017).
- International GNSS Service. *2nd Data reprocessing campaign guidelines* <http://acc.igs.org/reprocess2.html> (2014).
- Dow, J. M., Neilan, R. E. & Rizos, C. The international GNSS service in a changing landscape of global navigation satellite systems. *J. Geodesy* **83**(3–4), 191–198 (2009).
- Serpelloni, E., Faccenna, C., Spada, G., Dong, D. & Williams, S. D. Vertical GPS ground motion rates in the Euro-Mediterranean region: New evidence of velocity gradients at different spatial scales along the Nubia-Eurasia plate boundary. *J. Geophys. Res.* **118**(11), 6003–6024 (2013).
- Devoti, R. *et al.* A combined velocity field of the Mediterranean region. *Ann. Geophys.* **60**(2), 0215 (2017).
- Schmid, R., Rothacher, M., Thaller, D. & Steigenberger, P. Absolute phase center corrections of satellite and receiver antennas. *GPS solutions* **9**(4), 283–293 (2005).

16. Schmid, R., Steigenberger, P., Gendt, G., Ge, M. & Rothacher, M. Generation of a consistent absolute phase-center correction model for GPS receiver and satellite antennas. *J. Geodesy* **81**, 781–798 (2007).
17. Petrie, E. J., King, M. A., Moore, P. & Lavallée, D. A. Higher-order ionospheric effects on the GPS reference frame and velocities. *J. Geophys. Res.* **115**(B3), B03417 (2010).
18. Boehm, J., Werl, B. & Schuh, H. Troposphere mapping functions for GPS and very long baseline interferometry from European centre for medium range weather forecasts operational analysis data. *J. Geophys. Res.* **111**, B02406 (2006).
19. Lyard, F., Lefevre, F., Letellier, T. & Francis, O. Modelling the global ocean tides: Modern insights from fes2004. *Ocean Dyn.* **56**, 394–415 (2006).
20. International GNSS Service. *IGb08 sinex file* <ftp://igs.org/pub/station/coord/IGb08.snrx> (2012).
21. Dong, D., Herring, T. A. & King, R. W. Estimating regional deformation from a combination of space and terrestrial geodetic data. *J. Geodesy* **72**(4), 200–214 (1998).
22. Dong, D., Fang, P., Bock, Y., Cheng, M. K. & Miyazaki, S. I. Anatomy of apparent seasonal variations from GPS-derived site position time series. *J. Geophys. Res.* **107**(B4), ETG-9 (2002).
23. International GNSS Service. IGS core stations list. ftp://ftp.igs.org/pub/station/coord/IGb08_core.txt (2012).
24. Bertiger, W. *et al.* Single receiver phase ambiguity resolution with GPS data. *J. Geodesy* **84**, 327–337 (2010).
25. Bar-Sever, Y. E., Kroger, P. & Borjesson, J. Estimating horizontal gradients of tropospheric path delay with a single GPS receiver. *J. Geophys. Res.* **103**(B3), 5019–5035 (1998).
26. Kedar, S., Hajj, G. A., Wilson, B. D. & Heflin, M. B. The effect of the second order GPS ionospheric correction on receiver positions. *Geophys. Res. Lett.* **30**(16), 1829 (2003).
27. Métois, M. *et al.* Insights on continental collisional processes from GPS data: Dynamics of the peri-adriatic belts. *J. Geophys. Res.* **120**, 8701–8719 (2015).
28. Wdowinski, S., Bock, Y., Zhang, J., Fang, P. & Genrich, J. Southern California permanent GPS geodetic array: Spatial filtering of daily positions for estimating coseismic and postseismic displacements induced by the 1992 Landers earthquake. *J. Geophys. Res.* **102**, 18057–18070 (1997).
29. Palano, M. *et al.* Geopositioning time series from offshore platforms in the Adriatic Sea. *PANGAEA* <https://doi.org/10.1594/PANGAEA.914358> (2020).
30. Wu, D., Yan, H. & Shen, Y. TSAAnalyzer, a GNSS time series analysis software. *GPS Solutions* **21**(3), 1389–1394 (2017).
31. Wu, D., Yan, H. & Shen, Y. TSAAnalyzer, a GNSS time series analysis software. *The GPS Toolbox* <https://geodesy.noaa.gov/gps-toolbox/TSAAnalyzer.htm> (2017).
32. Abramowitz, M. & Stegun, I. A. *Handbook of Mathematical Functions with Formulas, Graphs, and Mathematical Tables* (National Bureau of Standards Applied Mathematics Series 55, Tenth Printing, 1972).
33. Cheloni, D. *et al.* Geodetic model of the 2016 Central Italy earthquake sequence inferred from InSAR and GPS data. *Geophys. Res. Lett.* **44**, 6778–6787 (2017).
34. Herring, T. A. *et al.* Plate Boundary Observatory and related networks: GPS data analysis methods and geodetic products. *Rev. Geophys.* **54**(4), 759–808 (2016).
35. Altamimi, Z., Laurent, M. & Xavier, C. ITRF2008 plate motion model. *J. Geophys. Res.* **117**, B7 (2012).
36. Palano, M. On the present-day crustal stress, strain-rate fields and mantle anisotropy pattern of Italy. *Geophys. J. Int.* **200**(2), 969–985 (2015).
37. Cushman-Roisin, B., Malačić, V., & Gačić, M. Tides, Seiches and Low-Frequency Oscillations. in *Physical Oceanography of the Adriatic Sea* (eds. Cushman-Roisin, B., Gacic, M., Poulain, P.-M. & Artegiani, A.) Ch. 7 (Springer, Dordrecht, 2001).
38. Poulain, P. M. Adriatic Sea surface circulation as derived from drifter data between 1990 and 1999. *J. Marine Syst.* **29**(1–4), 3–32 (2001).

Acknowledgements

This research was financed by the Italian Economic Development Ministry in the “CLYPEA-Innovation Network for Future Energy” framework, “subsoil deformations” project. We thank Gilberto Dialuce (General Director of DG ISSEG of the Italian Economic Development Ministry) and Franco Terlizze (Director of DGS UNMIG of the Italian Economic Development Ministry) who designed and encouraged the CLYPEA project, creating a successful synergy between INGV, University of Bologna, RSE, Polytechnic of Turin, La Sapienza University, CNR-IGAG, CNR-IREA and Emilia Romagna Region. We thank Eni S.p.A. for providing GNSS data; in particular, we thank Gianfranco Roncari, Roberto Miandro, Carolina Dacome and Stefano Mantica. We are also grateful to Luisa Perini and Paolo Severi for fruitful discussions. Encouragement and continuous support by Carlo Doglioni, Andrea Morelli and Claudio Chiarabba were greatly appreciated.

Author contributions

M.P., G.P., E.S., R.D., N.D. and S.G. conceived and designed the research. M.P., E.S., F.S., L.A., R.D., N.D., S.G., L.P., L.T., P.M., G.P. and F.R. processed the GNSS data. M.P. wrote most of the manuscript. All the authors discussed the contents and approved the final manuscript.

Competing interests

The authors declare no competing interests.

Additional information

Supplementary information is available for this paper at <https://doi.org/10.1038/s41597-020-00705-w>.

Correspondence and requests for materials should be addressed to M.P. or G.P.

Reprints and permissions information is available at www.nature.com/reprints.

Publisher’s note Springer Nature remains neutral with regard to jurisdictional claims in published maps and institutional affiliations.



Open Access This article is licensed under a Creative Commons Attribution 4.0 International License, which permits use, sharing, adaptation, distribution and reproduction in any medium or format, as long as you give appropriate credit to the original author(s) and the source, provide a link to the Creative Commons license, and indicate if changes were made. The images or other third party material in this article are included in the article's Creative Commons license, unless indicated otherwise in a credit line to the material. If material is not included in the article's Creative Commons license and your intended use is not permitted by statutory regulation or exceeds the permitted use, you will need to obtain permission directly from the copyright holder. To view a copy of this license, visit <http://creativecommons.org/licenses/by/4.0/>.

The Creative Commons Public Domain Dedication waiver <http://creativecommons.org/publicdomain/zero/1.0/> applies to the metadata files associated with this article.

© The Author(s) 2020